

https://doi.org/10.1070/QEL17170

Effect of frequency detuning on Brillouin lasing in microcavities

D.A. Korobko, I.O. Zolotovskii, V.V. Svetukhin, A.V. Zhukov,
A.N. Fomin, K.V. Borisova, A.A. Fotiadi

Abstract. **We have theoretically investigated Brillouin lasing in microcavities in the case when the Brillouin shift and the intermode spacing of the microcavity do not coincide. It is shown that, despite the rise of the lasing threshold, a significant increase in the Brillouin signal intensity can be achieved in this case compared to the resonance one. A necessary condition for this effect is to select an optimal value of detuning of the pump radiation frequency from the frequency of the corresponding microcavity mode. The result of increasing the lasing threshold is also a narrowing of the Brillouin signal lasing range in the nonresonant case, which leads to a decrease in the signal noise level provided the detuning value is optimally selected. Analytical calculations are confirmed by the results of numerical modelling.**

Keywords: *narrow-band lasers, SBS lasers, microcavities, Brillouin shift.*

1. Introduction

The development of narrow-band low-noise laser sources is one of the central tasks of modern photonics [1–3]. The scope of their applications is very wide: it includes, for example, distributed fibre monitoring [4, 5], precision spectroscopy [6], optical communications [7], nonlinear frequency conversion schemes [8] and microwave photonics [9]. Among the most available and studied methods for narrowing the laser linewidth, we should note the use of distributed feedback (DFB) configurations [10, 11], including lasers integrated with external cavities or microcavities (MCs) [12–14]. The use of such configurations makes it possible to narrow the linewidth of standard semiconductor DFB lasers down to kilohertz [15].

However, recent decades have seen a rapid progress in another direction related to the development of narrow-band lasers based on stimulated Brillouin scattering (SBS). The characteristic features of such lasers are a low lasing threshold and a narrow gain linewidth (tens of MHz) [16]. Such a narrow linewidth, which does not exceed the intermode spacing, makes it possible to develop single-frequency SBS fibre lasers with a cavity length of about 10 m [17, 18]. In recent years, there has been a fundamental breakthrough in the study of SBS lasers, related to the transition from fibre technologies to integrated photonics technologies [19]. SBS lasers in an integrated optical design retain their basic properties, are less expensive and more compact, which is important for use in sensors, large data processing systems, atomic clocks, etc. [20]. Recently, an SBS laser based on a ring waveguide with a Si_3N_4 structure was demonstrated, which allows preserving all the advantages of this type of laser translated to an optoelectronic platform [21]. It is also important that the optoelectronic design allows the use of a number of materials with an increased SBS gain (waveguides based on silicon, chalcogenide glasses, etc.) [22–25].

Effective SBS lasing in an MC is provided by adjusting the resonator intermode frequency spacing to the Brillouin frequency shift, which can be implemented by accurate setting the dimensions during the manufacturing process. Modern technologies allow the MC sizes to be controlled, ensuring the accuracy of the free spectral range (FSR) on the order of 1 MHz, provided that its value is equal to the Brillouin shift Ω_B [with $\Omega_B/(2\pi) \sim 10$ GHz] [25]. This accuracy does not exclude, however, the need to take into account the effects associated with the presence of FSR detuning of the resonator from the Brillouin shift value. Indeed, both parameters (FSR and Ω_B) depend, in different ways, on the pump wavelength; in addition, the impact of external factors (temperature, deformation, etc.) should be taken into account. Allowance for these effects is also necessary when solving specific problems in physics of SBS lasers (for example, for tuning the laser frequency, tuning the generation of the Brillouin comb spectrum [26], as well as in sensor applications [27]).

The aim of this work is to describe the effects that arise in MC-based SBS lasers in the case when the Brillouin shift frequency and the spectral spacing between the pump modes and the Stokes wave modes in the resonator, which is a multiple of the free spectral parameter FSR, coincide inaccurately. The generality of the approaches under consideration does not exclude their application to any type of SBS lasers with a sufficiently short (less than 1 m) resonator, i.e., generating in the single-frequency regime. Nevertheless, we consider the MC as the main object of research in the composition of integrated optical platforms. It is also important to note that the generation of Stokes components of the second and higher orders is excluded from consideration, which can technically be done using an additional MC-associated filter.

D.A. Korobko, I.O. Zolotovskii, A.V. Zhukov, A.N. Fomin, K.V. Borisova Ulyanovsk State University, ul. L. Tolstogo 42, 432700 Ulyanovsk, Russia; Scientific-Manufacturing Complex 'Technological Centre', pl. Shokina 1, stroenie 7, Zelenograd, 124498 Moscow, Russia; e-mail: korobkotam@rambler.ru;
V.V. Svetukhin Scientific-Manufacturing Complex 'Technological Centre', pl. Shokina 1, stroenie 7, Zelenograd, 124498 Moscow, Russia;
A.A. Fotiadi Ulyanovsk State University, ul. L. Tolstogo 42, 432700 Ulyanovsk, Russia; Scientific-Manufacturing Complex 'Technological Centre', pl. Shokina 1, stroenie 7, Zelenograd, 124498 Moscow, Russia; University of Mons (Belgium), 31, blvd. Dolez, B-7000 Mons, Belgium

Received 22 October 2019
Kvantovaya Elektronika **50** (3) 284–290 (2020)
Translated by M.A. Monastyrskiy

2. Basic relations

We consider the standard scheme of an MC-based Brillouin laser pumped by a cw laser (Fig. 1a). The MC is tunnelly coupled to a waveguide for laser pump radiation with frequency ω_S, which excites a forward wave with an amplitude $A_F(t)$ at a frequency ω_F. When a forward wave is scattered by existing thermal density fluctuations (with an equilibrium value ρ_0), a backward (Brillouin) wave is generated with an amplitude $A_B(t)$ and a frequency ω_B. Then, with the development of the Brillouin process, an acoustic density wave with an oscillation amplitude $\rho(t)$ is excited.

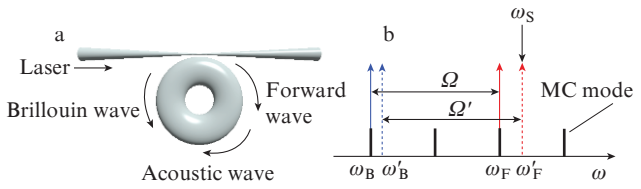

Figure 1. Schemes for (a) Brillouin lasing in the microcavity and (b) tuning the frequencies of the forward, backward, and acoustic waves when detuning the pump frequency from the frequency of the microcavity mode.

The amplitudes of interacting waves in the MC are related by a system of equations [28]

$$\begin{aligned}
\frac{\partial A_F}{\partial t} &= -\frac{A_F}{2\tau_F} - i\frac{\gamma_e\omega_F}{4n_0^2\rho_0}\Lambda_F A_B\rho \\
&\quad + \sqrt{\frac{1}{\tau_{ext}}}S\exp[i(\omega_S-\omega_F)t], \\
\frac{\partial A_B}{\partial t} &= -\frac{A_B}{2\tau_B} - i\frac{\gamma_e\omega_B}{4n_0^2\rho_0}\Lambda_B A_F\rho^*, \\
\frac{\partial \rho}{\partial t} &= i\frac{\Omega_B^2-\Omega^2}{2\Omega}\rho - \frac{\Gamma}{2}\rho - i\frac{\varepsilon_0\gamma_e}{4\Omega}\frac{\ell_\rho^2}{R^2}\Lambda_\rho A_F A_B^*.
\end{aligned} \tag{1}$$

Here, ω_F is the MC mode frequency closest to the pump frequency ω_S; Ω is the acoustic wave frequency; Ω_B is the frequency corresponding to the gain maximum [i.e., $\Omega_B/(2\pi)$ is the Brillouin shift]; γ_e is the electrostriction constant; n_0 is the refractive index of the MC material; ρ_0 is the equilibrium value; Γ is the attenuation parameter; and Λ_F, Λ_B, and Λ_ρ are the overlap integrals [16] that depend on the transverse distribution of the mode fields. When deriving the third equation of system (1), we assumed that the fields of the forward and backward waves have the form of a fundamental mode in the transverse distribution. Given that the waves propagate near the external boundary of the resonator, the radius of the mode trajectory is assumed to be equal to the radius R of the resonator. The phase matching conditions are written as $\Omega = \omega_F - \omega_B$, i.e., the difference between the forward and backward wave frequencies is equal to the frequency of the acoustic wave, and $\ell_\rho = \ell_F + \ell_B$, i.e., its angular momentum is equal to the sum of the moments of the forward and backward waves. For simplicity, which does not fundamentally change the solution to the problem in question, we set $\Lambda_F = \Lambda_B = \Lambda_\rho = 1/2$. This is justified in particular by the fact that the mode numbers of the forward and backward waves are close [28].

The values τ_F and τ_B correspond to the lifetimes of the forward and backward waves, which, naturally, are associated with the MC energy losses. These losses can be divided into two parts: material losses characterised by the times τ_{F0} and τ_{B0}, and output waveguide coupling losses characterised by the time τ_{ext}. For the forward and backward waves, we have the relations

$$\frac{1}{\tau_F} = \frac{1}{\tau_{F0}} + \frac{1}{\tau_{ext}},$$

$$\frac{1}{\tau_B} = \frac{1}{\tau_{B0}} + \frac{1}{\tau_{ext}}.$$

If we denote the power amplitude of the injected pump as S, then the value of $|S|^2$ is proportional to the pump power; $|A_F|^2$ and $|A_B|^2$ are proportional to the energies of the corresponding waves [29]. Then the relation describing the energy conservation in the MC takes the form

$$\frac{|A_B|^2}{\tau_B} + \frac{|A_F|^2}{\tau_{F0}} = |S|^2 - |T|^2, \tag{2}$$

where $|T|^2$ is the power passed through the MC in the forward direction.

Detuning the pump wave frequency from the MC frequency leads to the fact that a stationary solution to Eqns (1) can only be obtained for waves with frequency detunings $\sigma_F = \omega_S - \omega_F$, $\sigma_B = \omega'_B - \omega_B$, $\sigma_\rho = \Omega' - \Omega$ [for amplitudes, the expression $A'_k = A_k\exp(-i\sigma_k t)$ is valid]. The realisation of phase matching requires the condition $\sigma_F = \sigma_B + \sigma_\rho$ to be fulfilled. Given that the complex amplitudes of interacting waves have the form $A'_F = |A'_F|\exp(i\varphi_F)$, $A'_B = |A'_B|\exp(i\varphi_B)$, and $\rho' = |\rho'|\exp(i\varphi_\rho)$, Eqns (1) can be expressed as (hereafter the primes are omitted)

$$\begin{aligned}
\frac{\partial|A_F|}{\partial t} &= \frac{|A_F|}{2\tau_F} + \frac{\gamma_e\omega_0}{8n_0^2\rho_0}|A_B||\rho|\sin(\varphi_\rho+\varphi_B-\varphi_F) \\
&\quad + \sqrt{\frac{1}{\tau_{ext}}}|S|\cos(\varphi_S-\varphi_F), \\
\frac{\partial\varphi_F}{\partial t} &= -\sigma_F - \frac{\gamma_e\omega_0}{8n_0^2\rho_0}\frac{|A_B||\rho|}{|A_F|}\cos(\varphi_\rho+\varphi_B-\varphi_F) \\
&\quad + \sqrt{\frac{1}{\tau_{ext}}}\frac{|S|}{|A_F|}\sin(\varphi_S-\varphi_F), \\
\frac{\partial|A_B|}{\partial t} &= -\frac{|A_B|}{2\tau_B} + \frac{\gamma_e\omega_0}{8n_0^2\rho_0}|A_F||\rho|\sin(\varphi_F-\varphi_B-\varphi_\rho), \\
\frac{\partial\varphi_B}{\partial t} &= -\sigma_B - \frac{\gamma_e\omega_0}{8n_0^2\rho_0}\frac{|A_F||\rho|}{|A_B|}\cos(\varphi_F-\varphi_B-\varphi_\rho), \\
\frac{\partial|\rho|}{\partial t} &= -\frac{\Gamma}{2}|\rho| + \frac{\varepsilon_0\gamma_e}{8\Omega}\frac{\ell_\rho^2}{R^2}|A_F||A_B|\sin(\varphi_F-\varphi_B-\varphi_\rho), \\
\frac{\partial\varphi_\rho}{\partial t} &= -\sigma_\rho + \frac{\Omega_B^2-\Omega^2}{2\Omega} \\
&\quad - \frac{\varepsilon_0\gamma_e}{8\Omega}\frac{\ell_\rho^2}{R^2}\frac{|A_F||A_B|}{|\rho|}\cos(\varphi_F-\varphi_B-\varphi_\rho).
\end{aligned} \tag{3}$$

Standard simplification is also accepted here: due to the proximity of ω_F to ω_B, we may assume that $\omega_B \approx \omega_F = \omega_0$.

3. Analytical calculation

Analysis of solutions to system (3) for various detunings $\Omega_B - \Omega$ is the main part of this work. Considering the steady-state regime established after the transition processes (the derivatives on the left-hand side are equal to zero), we note that the stationary values of the energies of forward and backward waves can be easily found:

$$|A_F|^2 = \frac{16 n_0 \rho_0 \Gamma \Omega R^2}{\tau_B \varepsilon_0 \gamma_e^2 \omega_0 \ell_\rho^2} \frac{1}{\sin^2(\varphi_F - \varphi_B - \varphi_\rho)},$$
$$|A_B|^2 = \frac{2\tau_B}{\sqrt{\tau_{ext}}} |S||A_F| \cos(\varphi_S - \varphi_F) - \frac{\tau_B}{\tau_F} |A_F|^2. \quad (4)$$

It can be seen that in the steady-state lasing regime, the forward wave energy does not depend on the pump power, but is determined by the resonator parameters and the relationship between the phases of interacting waves. In other words, when the threshold is reached, the forward wave energy is captured at a given level. With a further increase in external pumping, all its energy passed into the MC is transferred to the backward wave. The second relation in (4) is a different formulation of the law of energy conservation (2). The equivalence between them follows from the relation $A_F/\sqrt{\tau_{ext}} = S + T$ [29]. We represent equation (2) in the form describing the relationship between the pump power and the Brillouin wave power $|A_B|^2/\tau_{ext}$ coupled out from the MC:

$$\frac{|A_B|^2}{\tau_{ext}} = \frac{\tau_B}{\tau_{ext}} \left(|S|^2 - |T|^2 - \frac{|A_F|^2}{\tau_{F0}} \right). \quad (5)$$

In (5), the τ_B/τ_{ext} value can be identified as a lasing efficiency parameter, while $|A_F|^2/\tau_{F0}$ characterises its threshold power.

To study the lasing parameters in the presence of frequency detunings, we consider the energies of interacting waves as a function of the detuning σ_F between the pump and forward wave frequencies in the MC. In particular, it follows from system (3) and phase matching conditions that

$$\sigma_B = \frac{\sigma_F - (\Omega_B^2 - \Omega^2)/(2\Omega)}{1 + \Gamma\tau_B},$$
$$\sigma_\rho = \frac{\sigma_F \Gamma\tau_B + (\Omega_B^2 - \Omega^2)/(2\Omega)}{1 + \Gamma\tau_B}, \quad (6)$$

i.e., the value of σ_F and the difference between the Brillouin shift and the intermode spacing $\Omega_B - \Omega$ determine the frequency shift of the backward wave. Detunings, in turn, affect the relationship between the phases of interacting waves. Indeed, considering the case $\Omega_B = \Omega$, we note that, at a zero pump frequency detuning, the relation $\sigma_B = \sigma_\rho = 0$ is satisfied, which implies the phase matching condition in the steady-state regime: $\varphi_F - \varphi_B - \varphi_\rho = \pi/2$ and $\varphi_S - \varphi_F = 0$. In the presence of any detuning, the phase matching point shifts, and this results in a shift in the steady state and a change in the wave energies. In particular, from system (3) we can obtain the relation:

$$\sin^2(\varphi_F - \varphi_B - \varphi_\rho) = \frac{1}{1 + 4\tau_B^2 \sigma_B^2}.$$

Using it, for the steady-state regime, we obtain an expression for the energy of the forward wave and an equation that implicitly determines the energy of the backward wave as a function of the detunings:

$$|A_F|^2 = \frac{g}{\tau_B} \left\{ 1 + \left[\frac{2(\sigma_F - \Delta)\tau_B}{1 + \Gamma\tau_B} \right]^2 \right\},$$
$$|A_B|^2 = \sqrt{\frac{4g\tau_B}{\tau_{ext}} [1 + (2\sigma_B\tau_B)^2]} S \cos(\varphi_S - \varphi_F) - \frac{\tau_B}{\tau_F} |A_F|^2,$$
$$\cos(\varphi_S - \varphi_F) = \left| \frac{\sqrt{1 + (2\sigma_B\tau_B)^2}}{2\tau_F} + \frac{\frac{|A_B|^2}{2g}}{\sqrt{1 + (2\sigma_B\tau_B)^2}} \right| \times \left\{ [1 + (2\sigma_B\tau_B)^2] \left[\sigma_F^2 + \left[\frac{1}{2\tau_F} \right]^2 \right] + \frac{|A_B|^2}{2g} \left[\frac{1}{\tau_F} - 4\sigma_F\sigma_B\tau_B \right] + \frac{|A_B|^4}{4g^2} \right\}^{-1/2}, \quad (7)$$

where $g = 16\rho_0\Gamma\Omega n_0^2 R^2/(\omega_0 \varepsilon_0 \gamma_e^2 \ell^2)$; and $\Delta = (\Omega_B^2 - \Omega^2) \times (2\Omega)^{-1}$. Let us analyse the obtained relations. The values of the system parameters used for calculations (given below) correspond to a quartz disk (or spherical) cavity with a radius of 2.8 mm and a mode area of 25 μm^2 [28].

$\tau_F = \tau_B$/s	$(2\pi \times 2 \times 10^6)^{-1}$
τ_{ext}/s	$(2\pi \times 1.33 \times 10^6)^{-1}$
Γ/s^{-1}	$2\pi \times 15.64 \times 10^6$
Ω_B/s^{-1}	$2\pi \times 11.55 \times 10^9$
γ_e	1.5
n_0	1.5
ρ_0/kg m^{-3}	2200
ℓ/R/m^{-1}	1.22×10^7

Consider pumping with $\lambda = 1550$ nm, corresponding to $\omega_0 = 1.22 \times 10^{15}$ s^{-1}. The pump power of 1 mW under these conditions corresponds to the normalisation $|S|^2 = 2.3 \times 10^{20}$ W m^{-2} F^{-1}.

First, we consider the standard situation when the Brillouin shift is exactly equal to the spectral spacing between the two MC modes, i.e., $\Delta = 0$. Figure 2a shows the dependences of the forward and backward wave energies on the corresponding detunings. When the pump frequency detuning is increased, the forward wave energy increases as $\propto \sigma_F^2$, symmetrically relative to the change in the detuning sign, while the energy $|A_F|^2$, in accordance with (4), does not depend on the pump level. At low pump powers P_{pump} and close-to-zero detuning σ_F, threshold values of the forward wave energy are minimal, and the backward wave is also generated in a narrow range $\sigma_B \to 0$. A consequence of expression (6), which is important for attaining narrowband lasing, is that the region of σ_B variation is $(1 + \Gamma\tau_B)$ times narrower than the linewidths located between the threshold points σ_F. As the pump level increases, both the energy and the generation linewidth of the backward wave increase. The width of the interthreshold band σ_F is also increased. We should note a relatively 'flat' dependence of the backward wave energy $|A_B|^2$ on the detuning magnitude.

Next, we compare the situation considered with the case when, for some reasons, the Brillouin shift exceeds the intermode spacing, $\Omega_B > \Omega$ (Fig. 2b). Under these conditions, the effect of frequency pulling is manifested [30], i.e., the shift of the detuning σ_B to the negative region, accompanied by an increase in σ_ρ. As can be seen from the figure, the detuning $\Delta/(2\pi) = 20$ MHz causes a shift of the Brillouin linewidth by 2.5–3 MHz. The dependence of the forward wave energy is

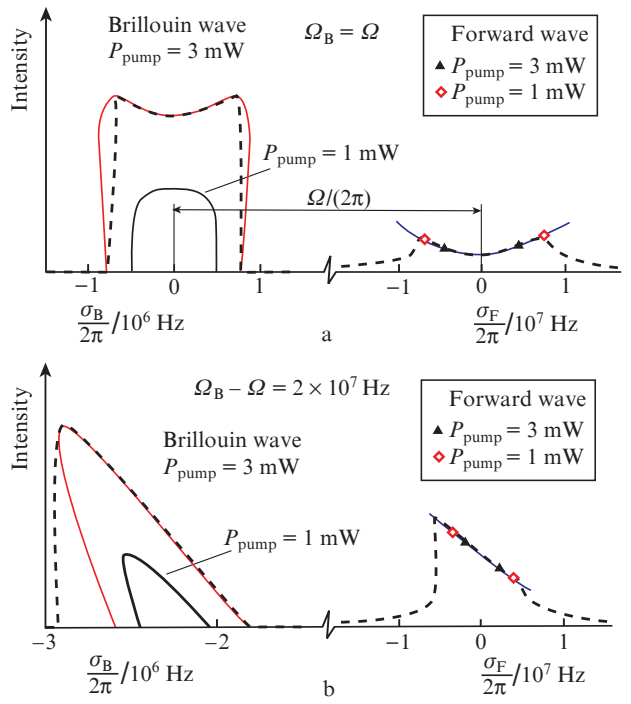

Figure 2. (a) Dependences of the backward (Brillouin) wave energy on the detuning σ_B in the steady-state lasing regime at different pump powers (left) and the forward wave energy on the detuning σ_F when the Brillouin shift coincides with the intermode spacing (right); (b) the same, but for the Brillouin shift detuning on the spacing between the MC modes $\Delta/(2\pi) = 20$ MHz. Symbols indicate the forward wave energy levels corresponding to the lasing threshold. Dashed lines are the results of numerical simulation of system (3) at $P_{pump} = 3$ mW. Pay attention to the difference in scales for σ_F and σ_B.

deformed, i.e. the minimum $|A_F|^2$ shifts to the point $\sigma_F = \Delta$, while the wave energy increases, and the width of the interthreshold band σ_F reduces significantly. Accordingly, the laser linewidth in the detuning range σ_B is narrowed. The dependence of the energy $|A_B|^2$ on the detuning is characterised by a wide bistability band, whose lower branch corresponds to unstable solutions. The maximum energy of the backward wave, due to pulling, lies in the region of the minimum allowable values of σ_B, limited by the condition $\cos(\varphi_S - \varphi_F) = 1$. Note that in a certain band of detunings σ_B (or, in other words, in a certain range of Δ) at a sufficiently high pump level, the maximum value of the backward wave energy increases relative to its value at resonance (for $\Delta = \sigma_B = \sigma_F = 0$). In particular, it follows from Fig. 2 that at $\Delta/(2\pi) = 20$ MHz and a pump power of 1 mW or higher, the maximum energy of the Brillouin wave increases compared to the fully resonant case. Assuming that the detuning Δ is sufficient for the pulling to exceed the characteristic losses, i.e., $\sigma_B > 1/\tau_B$, we can obtain the estimate for the parameters at which this effect occurs:

$$\frac{(2\sigma_B\tau_B - 1)}{2(\sigma_B\tau_B)^2} S > \frac{1}{\tau_F}\sqrt{\frac{g\tau_{ext}}{\tau_B}}.$$

4. Numerical simulation results

Consider the results obtained by numerical simulation of system (3). To describe the lasing dynamics, the third equation of system (1) should be supplemented with a free term $f(t)$ describing small fluctuations in thermal density (Langevin noise source). In its absence, as is easily seen, lasing is absent, since the initial conditions $A_B = \rho = 0$ do not change. For a source $f(t)$ that has a form of white noise, if the real and imaginary parts are equal, the expression $\{f(t)f^*(t)\} = C\delta(t'-t)$ is valid, where $C = kT\rho_0\Gamma/Vv^2$; k is the Boltzmann constant; V is the acoustic mode volume; and v is the speed of sound [31]. In the lasing regime, this noise term leads to fluctuations in the amplitude and phase of the interacting waves associated with the limiting laser linewidth. When it is 'disabled' in the lasing regime, the interacting waves become completely coherent. The simulation was performed using the fourth-order Runge–Kutta method for zero initial energies of interacting waves at various pump powers until stationary values were reached. (In the presence of a stochastic source, the average characteristics of the corresponding values are called stationary ones. Their true, dynamically changing, values differ only by the value of small stochastic fluctuations.)

First, we compare the simulation results with the analytical ones. Figure 2 shows the results of simulation with parameters corresponding to theoretical calculations at a pump power of 3 mW. It can be seen that they coincide with the results obtained in the analysis of relations (7). The only exception is the 'unstable' branches of the backward wave energy $|A_B|^2$, which are not observed in the simulation. In addition, the simulation results are extended to a range of σ_F values, in which the backward wave is not generated, i.e., a range where the forward wave energy is below the threshold.

Next, we consider the process of Brillouin lasing in the MC as a function of the pump level. As before, we start with the case of resonant pumping, $\Delta = 0$ (Fig. 3a). By scanning the detuning σ_F, we determine the relative MC transmittance $|T|^2/|S|^2$ using expression (2). For small $S \to 0$, we obtain the transmission corresponding to the MC spectrum, which is only determined by the values of τ_{F0} and τ_{ext} (dashed curve in Fig. 3a). As the pump power increases, the backward wave is excited, and its detuning σ_B is determined by σ_F [relation (6)]. Note that the simulation results also correspond to the analytical ones: as the pump level increases, the energy transfer into the backward wave grows with increasing the MC transmittance, and the forward wave energy in the region Brillouin lasing does not depend on the pump power.

Figure 3b shows the dependence of the output power of Brillouin radiation $|A_B|^2/\tau_{ext}$ on the pump power. It can be seen that at a zero detuning σ_F, the threshold lasing power is minimal. It can be easily expressed using (4):

$$|S_0|^2 = \frac{g\tau_{ext}}{4\tau_B\tau_F^2}.$$

The efficiency of differential lasing with increasing pump level is reduced in accordance with formula (5), since an increase in $|S|^2$ takes place simultaneously with an increase in transmittance $|T|^2$. As has been predicted by analytical calculations, the presence of the pump frequency detuning from the resonance leads to an increase in the lasing threshold. However, when the pump level increases, the output Brillouin power induced at nonzero detuning exceeds the value obtained at $\sigma_F = 0$. This also follows from relations (7) and Fig. 2a, where the energy level $|A_B|^2$ corresponding to the near-threshold detuning values σ_F is higher than that in the central part at $\sigma_F = 0$.

Next, by analogy with the above, consider the situation when the Brillouin shift exceeds the intermode spacing: $\Omega_B > \Omega$

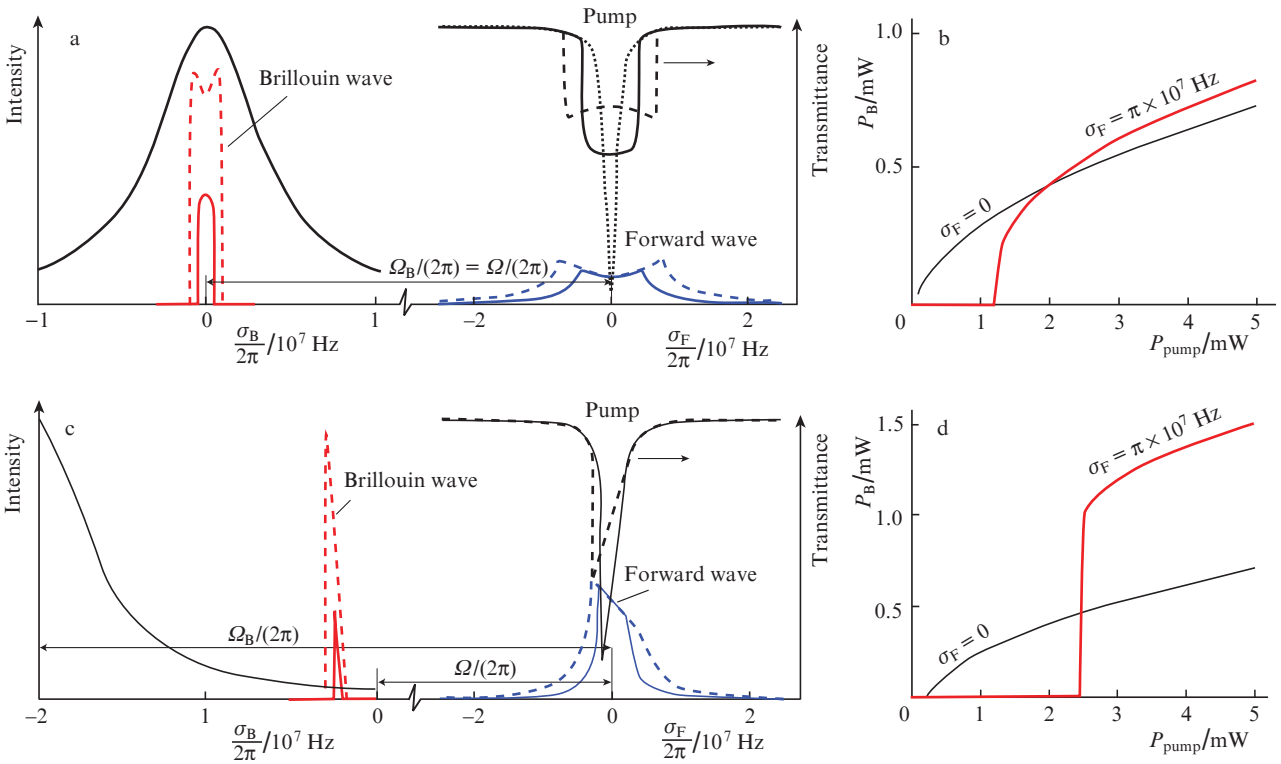

Figure 3. (a) Intensity of pump radiation passed into the MC and the MC transmittance as functions of the detuning σ_F (right), and also the backward wave intensity as a function of the detuning σ_B (left) at a pump power of 1 mW (solid curves) and 3 mW (dashed curves); (b) output power of Brillouin radiation as a functions of the pump power at various detuning values σ_F; (c and d, respectively) the same, when the detuning of the maximum Brillouin gain from the intermode spacing is $(\Omega_B - \Omega)/(2\pi) = 20$ MHz. In panels (a) and (b), the spectral spacing between the forward and backward waves coincides with the SBS shift; the dashed curve shows the cavity transmittance in the linear regime (without SBS lasing).

(Fig. 3c). Due to the pulling, there arises a characteristic transmittance asymmetry. The dependences of the forward and backward wave energies obtained in the simulation are also in accordance with analytical formulas (7), i.e., for a given pump power, the backward wave is generated in a narrower range of the detuning values σ_F than in the case $\Omega_B = \Omega$. The latter leads to a narrowing of the tuning range of Brillouin radiation σ_B?. These effects are explained by an increase in the lasing threshold, which is significantly higher than zero even for resonant pumping (at $\sigma_F = 0$). With an increase in the detuning σ_F, the threshold rises even more; however, the use of high-power pumping makes it possible to obtain Brillouin lasing with a power significantly greater than in the resonance case $\Omega_B = \Omega$ (Fig. 3d).

The regularities considered are illustrated in Fig. 4, which shows changes in the energies of the forward and backward waves as functions of the corresponding detuning values at different spectral spacings between the maximum Brillouin gain and the MC mode. We should note, in accordance with (6), the linear dependence of the detuning σ_B on the $\Omega_B - \Omega$ value. A rapid increase in the intensity of the forward wave when the linewidth ?σ_F in which Brillouin radiation is generated narrows, and a sharp jump in the backward wave intensity $|A_B|^2$ when the threshold is reached, also follow from the above reasoning. One can see from Fig. 4 that in a certain range of detuning values $\Omega_B - \Omega$, if the pump level is high enough, the maximum value of the backward wave energy increases compared to its value at resonance $\Delta = \sigma_B = \sigma_F = 0$. Note also that the pump level of 1 mW is sufficient to increase the maximum energy of the backward wave in the range of detuning values $0 < (\Omega_B - \Omega)/(2\pi) \leqslant 30$ MHz. The absolute maximum energy $|A_B|^2$ is fixed at $(\Omega_B - \Omega)/(2\pi) \leqslant 20$ MHz and the pump detuning is $\sigma_F \approx 2$ MHz. With a further increase in the Brillouin shift detuning from the intermode spacing, the backward wave energy decreases sharply. When the pump power is raised to 3 mW, the Brillouin signal generation range increases significantly; in the entire studied range of $0 < (\Omega_B - \Omega)/(2\pi) \leqslant 50$ MHz, the maximum energy of the backward wave exceeds its value at resonance. The absolute maximum energy of the Brillouin signal corresponds to the detuning $(\Omega_B - \Omega)/(2\pi) \approx 20$ MHz and the pump detuning $\sigma_F \approx 4$ MHz.

The noise characteristics of Brillouin lasing in the MC were also studied by numerical simulation. To this end, the spectral density of RIN of the backward wave

$$S(\omega) = \frac{2}{\langle |A_B|^2 \rangle^2} \int_{-\infty}^{+\infty} \langle \delta |A_B(t)|^2 \delta |A_B(t+\tau)|^2 \rangle \exp(i\omega\tau) \, d\tau$$

was characterised for different pump detuning values σ_F in two cases: when the Brillouin shift and the intermode spacing coincide and when the detuning is $(\Omega_B - \Omega)/(2\pi) = 20$ MHz. In the simulation, the pump power was chosen to be equal to 3 mW. The resonant case (Fig. 5a) is characterised by a 'flat' dependence of the backward wave intensity on the frequency detuning; therefore, the resulting weak dependence of the RIN spectral density on the detuning can be explained as follows: for $\sigma_F/(2\pi) \leqslant 5$ MHz, the RIN value in a wide frequency band (about 10 MHz) is approximately –140 dB Hz^{-1}. When detuning approaches its threshold values, the RIN value increases to –130 dB Hz^{-1} in the band up to 1 MHz.

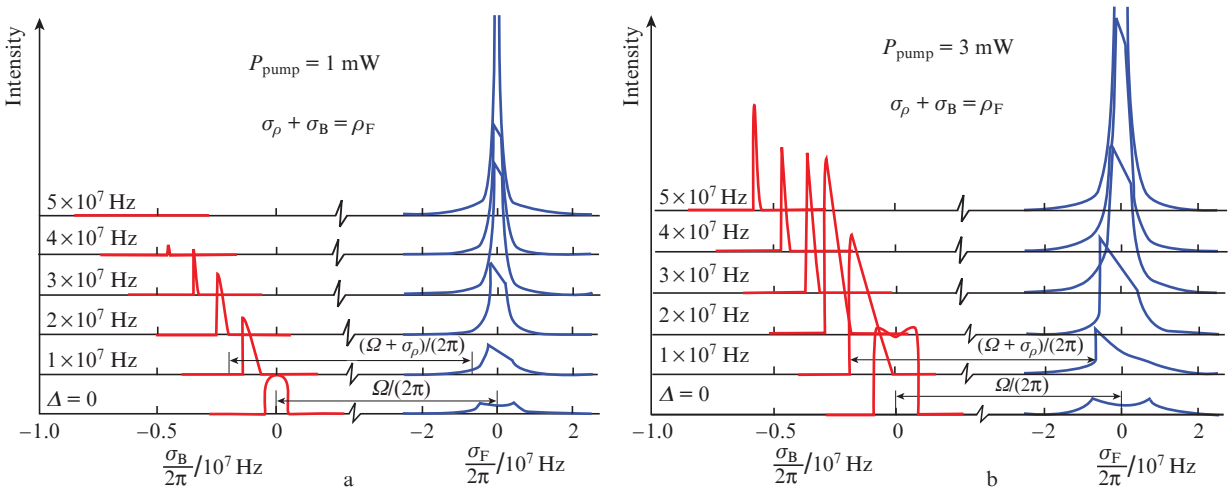

Figure 4. Dependences of the intensities of the forward and backward waves on the corresponding detunings σ_F and σ_B for various $\Delta = (\Omega_B - \Omega)/(2\pi)$ and pump powers of (a) 1 and (b) 3 mW. Pay attention to the difference in scales for σ_F and σ_B.

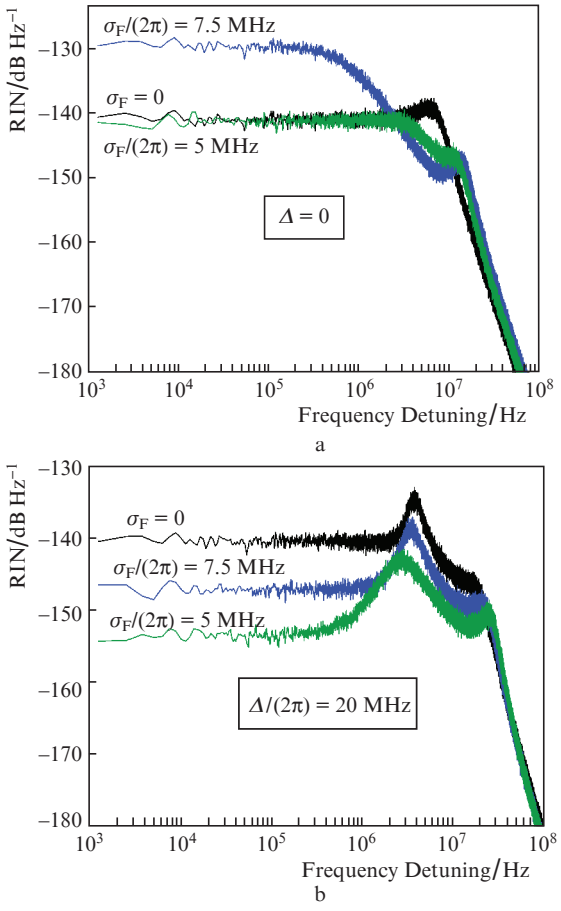

Figure 5. Results of numerical simulation. The spectral density of the relative noise intensity (RIN) of the Brillouin signal in the MC at different pump detunings i(a) n the case of the coincidence of the Brillouin shift and the intermode spacing and (b) at the detuning $(\Omega_B - \Omega)/(2\pi)$ = 20 MHz.

When determining RIN in the nonresonant case, one should pay attention to a remarkable fact – with the optimal choice of the pump frequency detuning, the noise characteristics of Brillouin lasing can be significantly improved (Fig. 5b). It can be seen that at $\sigma_F/(2\pi)$ = 5 MHz [at $(\Omega_B - \Omega)/(2\pi)$ = 20 MHz] the RIN value drops to about –155 dB Hz^{-1}. This can be explained by the narrowing of the Brillouin signal linewidth and the 'compression' of its response to fluctuations in the phase and amplitude of interacting waves during pump detuning that corresponds to the maximum intensity of the backward wave. Even despite the strong phase–amplitude coupling leading to the formation of a characteristic noise maximum near the frequencies of 2–4 MHz, the RIN level remains lower than in the resonance case in a wide frequency band of 1 kHz–50 MHz.

5. Conclusions

Based on the theoretical relationships, we have studied Brillouin lasing in an MC. Unlike most of the known works dedicated to this topic, the main attention was paid to studying the characteristics of the generated signal with a significant discrepancy between the Brillouin shift and the intermode spacing of the microcavity. It was shown that, despite an increase in the lasing threshold, which accompanies a shift in the gain maximum from the MC mode, the Brillouin signal intensity can be higher than that in the resonance case. A necessary condition for this effect is the selection of the optimal value for the pump frequency detuning from the frequency of the corresponding MC mode, while the consequence of increasing the lasing threshold – also narrowing the generation range of the Brillouin signal in the nonresonant case, which, provided this detuning is selected optimally, leads to a decrease in the signal noise level. The obtained analytical calculations are confirmed by numerical simulation data. The results of this work can be used not only for the design and analysis of experimental data of MC-based Brillouin lasers, but also for the development of microcavity sensors or other microwave photonics devices.

Acknowledgements. This work was supported by the Ministry of Higher Education and Science of the Russian Federation in the framework of the State Task of Scientific-Manufacturing Complex 'Technological Centre' for 2019.

References

1. Komljenovic T., Srinivasan S., Norberg E., Davenport M., Fish G., Bowers J.E. *IEEE J. Sel. Top. Quantum Electron.*, **21** (6), 214 (2015).
2. Matei D.G., Legero T., Häfner S., Grebing C., Weyrich R., Zhang W., Sterr U. *Phys. Rev. Lett.*, **118** (26), 263202 (2017).
3. Nikulin M.A., Babin S.A., Dmitriev A.K., Dychkov A.S., Kablukov S.I., Lugovoy A.A., Pecherskii Yu.Ya. *Quantum Electron.*, **39**, 906 (2009) [*Kvantovaya Elektron.*, **39**, 906 (2009)].
4. Kuznetsov A.G., Kharenko D.S., Babin S.A., Tsydenzhapov I.B., Shelemba I.S. *Quantum Electron.*, **47**, 967 (2017) [*Kvantovaya Elektron.*, **47**, 967 (2017)].
5. Bueno Escobedo J.L., Spirin V.V., López-Mercado C.A., Márquez Lucero A., Mégret P., Zolotovskii I.O., Fotiadi A.A. *Res. Phys.*, **7**, 641 (2017).
6. Chepurov S.V., Lugovoy A.A., Prudnikov O.N., Taichenachev A.V., Bagaev S.N. *Quantum Electron.*, **49**, 412 (2019) [*Kvantovaya Elektron.*, **49**, 412 (2019)].
7. Ip E., Lau A., Barros D., Kahn J. *Opt. Express*, **16**, 753 (2008).
8. Dontsova E.I., Kablukov S.I., Lobach I.A., Dostovalov A.V., Babin S.A., Gladyshev A.V., Dianov E.M. *Quantum Electron.*, **46**, 989 (2016) [*Kvantovaya Elektron.*, **46**, 989 (2016)].
9. Yao J. *J. Lightwave Technol.*, **27**, 314 (2009).
10. Napartovich A.P., Sukharev A.G. *Quantum Electron.*, **34**, 630 (2004) [*Kvantovaya Elektron.*, **34**, 630 (2004)].
11. Petermann K. *Laser Diode Modulation and Noise* (Springer Science & Business Media, 2012).
12. Liang W., Ilchenko V.S., Eliyahu D., Savchenkov A.A., Matsko A.B., Seidel D., Maleki L. *Nat. Commun.*, **6**, 7371 (2015).
13. Zolotovskii I.O., Korobko D.A., Fotiadi A.A., Panajotov K. *Quantum Electron.*, **47**, 871 (2017) [*Kvantovaya Elektron.*, **47**, 871 (2017)].
14. López-Mercado C.A., Spirin V.V., Bueno Escobedo J.L., Márquez Lucero A., Mégret P., Zolotovskii I.O., Fotiadi A.A. *Opt. Commun.*, **359**, 195 (2016).
15. Bueno Escobedo J.L., Spirin V.V., López-Mercado C.A., Mégret P., Zolotovskii I.O., Fotiadi A.A. *Res. Phys.*, **6**, 59 (2016).
16. Kobyakov A., Sauer M., Chowdhury D. *Adv. Opt. Photonics*, **2**, 1 (2010).
17. Smith S.P., Zarinetchi F., Ezekiel S. *Opt. Lett.*, **16**, 393 (1991).
18. Spirin V.V., López-Mercado C.A., Mégret P., Fotiadi A.A. *Laser Phys. Lett.*, **9**, 377 (2012).
19. Eggleton B.J., Poulton C.G., Rakich P.T., Steel M.J., Bahl G. *Nat. Photonics*, **1**, 13 (2019).
20. Diamandi H.H., Zadok A. *Nat. Photonics*, **13**, 9 (2019).
21. Gundavarapu S., Brodnik G.M., Puckett M., Huffman T., Bose D., Behunin R., Wu J., Qiu T., Pinho C., Chauhan N., Nohava J., Rakich P.T., Nelson K.D., et al. *Nat. Photonics*, **13**, 607 (2019).
22. Eggleton B.J., Luther-Davies B., Richardson K. *Nat. Photonics*, **5**, 141 (2011).
23. Eggleton B.J., Poulton C.G., Pant R. *Adv. Opt. Photonics*, **5**, 536 (2013).
24. Otterstrom N.T., Behunin R.O., Kittlaus E.A., Wang Z., Rakich P.T. *Science*, **360**, 1113 (2018).
25. Lee H., Chen T., Li J., Yang K.Y., Jeon S., Painter O., Vahala K.J. *Nat. Photonics*, **6**, 369 (2012).
26. Li J., Lee H., Vahala K.J. *Nat. Commun.*, **4**, 2097 (2013).
27. Li J., Suh M.G., Vahala K. *Optica*, **4**, 346 (2017).
28. Loh W., Papp S.B., Diddams S.A. *Phys. Rev. A*, **91**, 053843 (2015).
29. Haus H.A. *Waves and Fields in Optoelectronics* (New Jersey: Prentice-Hall, 1983).
30. Li J., Lee H., Chen T., Vahala K.J. *Opt. Express*, **20**, 20170 (2012).
31. Boyd R.W., Rzaewski K., Narum P. *Phys. Rev. A*, **42**, 5514 (1990).